Supplemental Text and Data for

Enhancement of Single Molecule Fluorescence Signals by Colloidal Silver Nanoparticles in Studies of Protein Translation

Shashank Bharill, Chunlai Chen, Benjamin Stevens, Jaskiran Kaur, Zeev Smilansky, Wlodek Mandecki, Ignacy Gryczynski, Zygmunt Gryczynski, Barry S. Cooperman and Yale E. Goldman*

Characterization of Wavelength-Shifted Background Emission of Silver Particles

Surfaces coated with colloidal particles and illuminated by visible laser light emitted luminescence, shifted to longer wavelengths. As such emission might interfere with detection of single fluorophores on a biological sample, we further characterized its relationship to the size of the silver particles and its spectral characteristics.

Particles at low density were illuminated by 532 nm laser light in TIRF mode and images were collected in orange (550 – 620 nm), and deep red (660 – 720 nm) emission channels on an EMCCD video camera (Fig. S1a and b). Backscattered 532 nm light (Fig. S1c, no emission filter, camera gain reduced to minimum) was imaged to detect the position of the silver particles.[1] Red-shifted intensity was detected in both of the long wavelength detector channels from some of the particles detected by scattering and AFM imaging (~15% and ~4%, respectively, Fig. S1).

We used a TIRF microscope integrated with an AFM system (Methods) to determine whether the size of the particles affected this emission. Regions of the slide were imaged by TIRF microscopy using 540 nm laser light and scanned by AFM (Fig. S1d and 1e respectively). The two images were scaled, registered with each other and merged using ImageJ and Matlab scripts. All of the spots producing red-shifted intensity could clearly be identified with objects in the AFM images (Fig. S1f), showing that the spots in both the orange and red emission channels originated at silver colloidal particles. Not all the silver particles detected by AFM produced appreciable background. The most intense spots were located at areas of the AFM image containing several silver particles or aggregates (Fig. S1d and e), as expected if larger silver colloids produce more red-shifted intensity than smaller ones. From size distributions of particles that produced appreciable background and the total population (Fig. S2a and b), we determined that 98% of the particles producing red-shifted background are 2.5×10^5 nm^3 or larger, although not all particles above this volume produced detectable background. The proportion of particles that produce red-shifted background intensity and their intensity depend strongly on the particle size (Fig. S2c).

Next, we determined the relative intensities from 50 nm and 85 nm diameter silver particles in the two camera fluorescence detector channels. Intensities were collected from 30 or more particles. The larger particles have ~3-fold more red-shifted background compared to the smaller ones when excited at either 532 nm or 640 nm with detection at 585 nm or 690 nm, respectively, and ~5-fold more luminosity when excited at 532 nm with detection at 690 nm (Table S1). Thus, the background from the larger particles is greater and extends to longer wavelengths than that from the smaller particles.

Supplementary Tables

Excitation/Emission Wavelengths	Small Colloids	Large Colloids
532 nm/585 nm	8437 ± 834	25152 ± 3306
640 nm/690 nm	6678 ± 783	18040 ± 3041
532 nm/690 nm	4023 ± 448	19610 ± 3183

TABLE S1. Average apparent luminosity values of small and large colloidal particles when illuminated by 532 or 640 nm laser light and detected in orange (585 ± 35 nm) or red (690 ± 30 nm) emission channels. Intensity measurements are means ± SEM of 30 or more particles. Values are means ± s.e.m.

	SURFACE	N	MEDIAN $x10^3$	MEAN $x10^3$	SD $x10^3$	BLEACHING TIME (s)	TOTAL PHOTONS $x10^5$	S/N	N/S	N_e/S
Cy3	GLASS	302	3.5	3.9	1.6	30	1.6	19	0.054	0.044
Cy3	COLLOIDS	115	23	26	12	31	6.9	29	0.035	0.017
Cy5	GLASS	113	4.4	4.6	1.6	33	2.7	20	0.049	0.039
Cy5	COLLOIDS	68	21	25	12	43	15	20	0.050	0.017

TABLE S2. Intensity distributions and noise of Cy3 and Cy5 labeled initiation complexes on glass and colocalized with small colloids. Mean and median intensity values are in camera A/D units, 10,000 ADUs = ~160 photons per pixel. Considering the widths of the intensity spots (σ_x and σ_y), total ADUs per molecule = 8.3-fold higher than the central intensity for Cy3 and 8.9-fold higher for Cy5. Bleaching time reports average recording time before photobleaching. Total photons collected were determined (using intensity, camera calibration and photobleaching time) from each recording and then averaged among traces. Signal to noise ratio (S/N) was calculated from Fourier transforms of the traces at 0.1 – 5 Hz. N/S is the reciprocal of S/N. N_e/S is the noise relative to signal intensity expected solely from Poisson counting statistics of the photoelectrons.

	SURFACE	N	MEDIAN $x10^3$	MEAN $x10^3$	SD $x10^3$	BLEACHING TIME	TOTAL PHOTONS $x10^5$	S/N	N/S	N_e/S
Cy5	GLASS	71	6.1	8.1	1.4	40	3.5	23.5	0.043	0.034
Cy5	COLLOIDS	128	41	40.5	12	29.5	17	13.4	0.075	0.013

TABLE S3. Intensity distributions and noise of Cy5 labeled initiation complexes on glass and colocalized with large colloids. Units and columns as in Table S2. Signal to noise ratios for plain glass are estimated.

Supplemental Figures

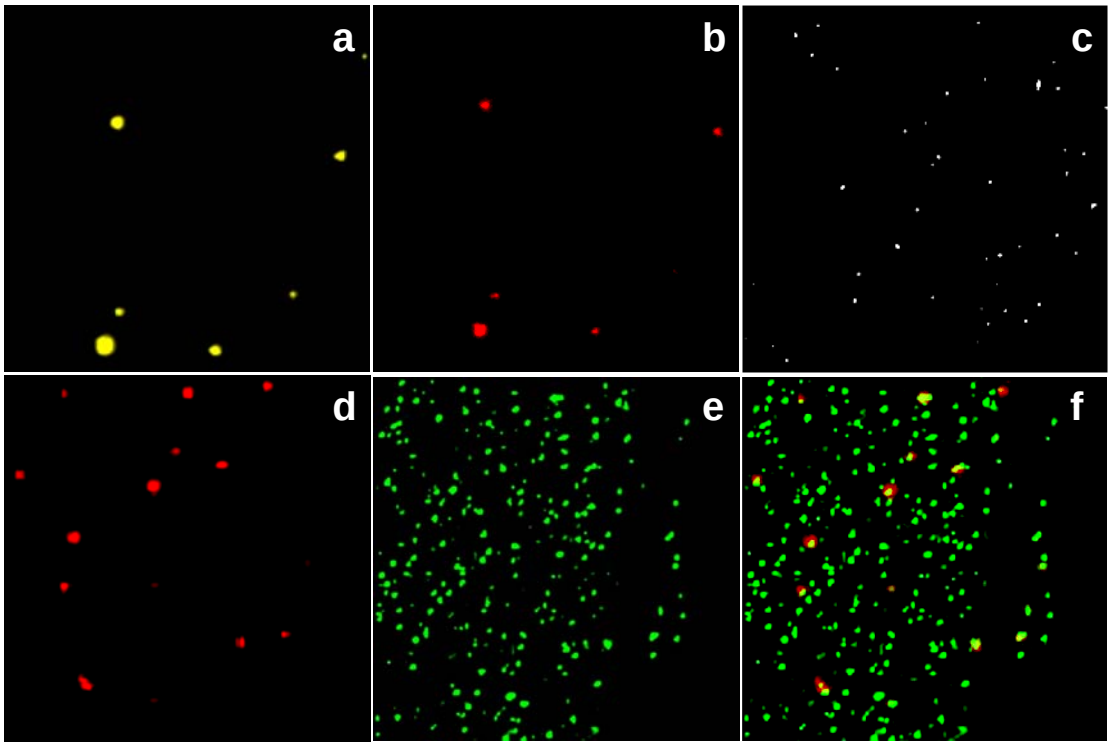

FIGURE S1. Imaging of small silver particles under 532 nm TIRF illumination. Luminescence images in the yellow-orange (560-620 nm) emission channel (a), deep red (660-720 nm) channel (b) and backscattered image (c) of small silver particles. Image in deep red channel (660-720 nm, d), AFM image (e) and merged luminescence-AFM image (f) of silver particles.

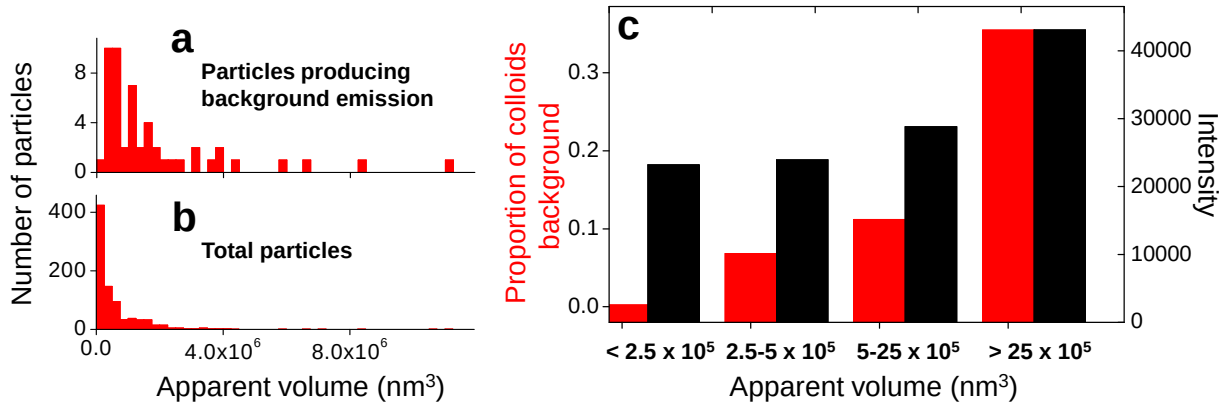

FIGURE S2. Apparent volume distributions of silver particles producing red-shifted background (a) and total silver particles (b) from the same region. (c) Dependence of proportion of silver particles giving background (red bars and red scale) and their intensities (black bars and black scale) on apparent volume of silver particles/aggregates.

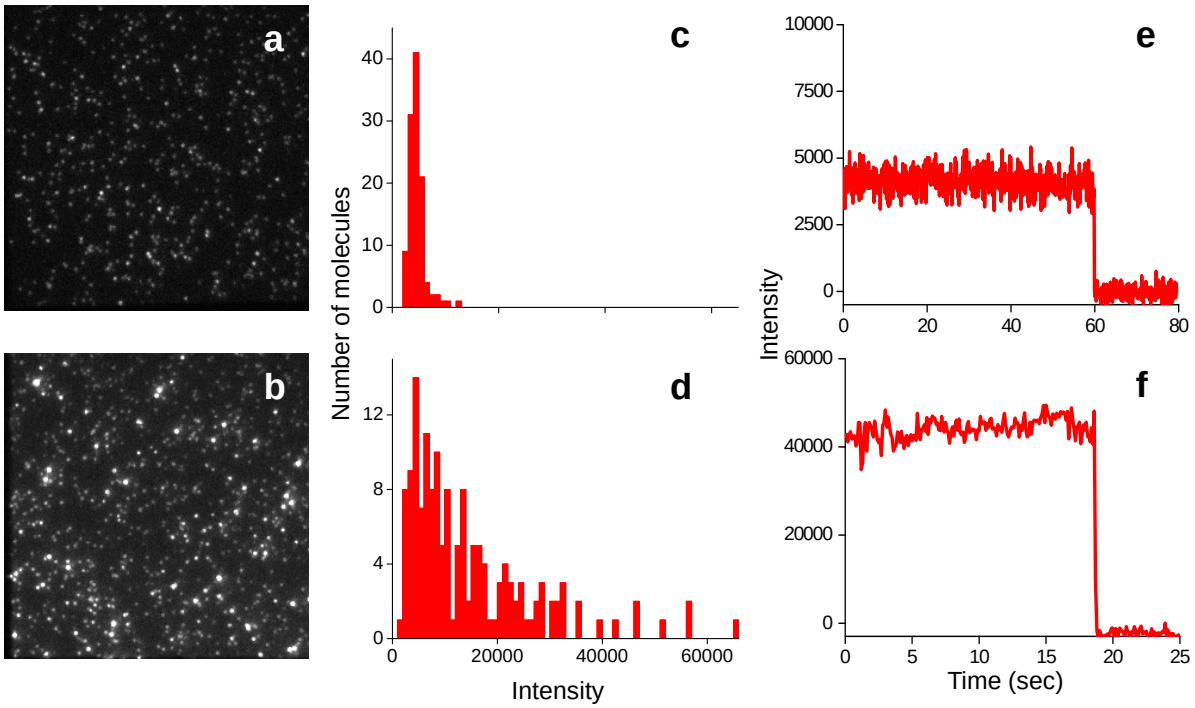

FIGURE S3. Comparison of Cy5 labeled initiation complexes (ICs) on the plain glass surface and small silver particle coated glass surface. Fluorescence images (a, b), intensity histograms (c, d), and single molecule traces (e, f), on plain glass (a, c, e) and on silver particle coated glass (b, d, f).

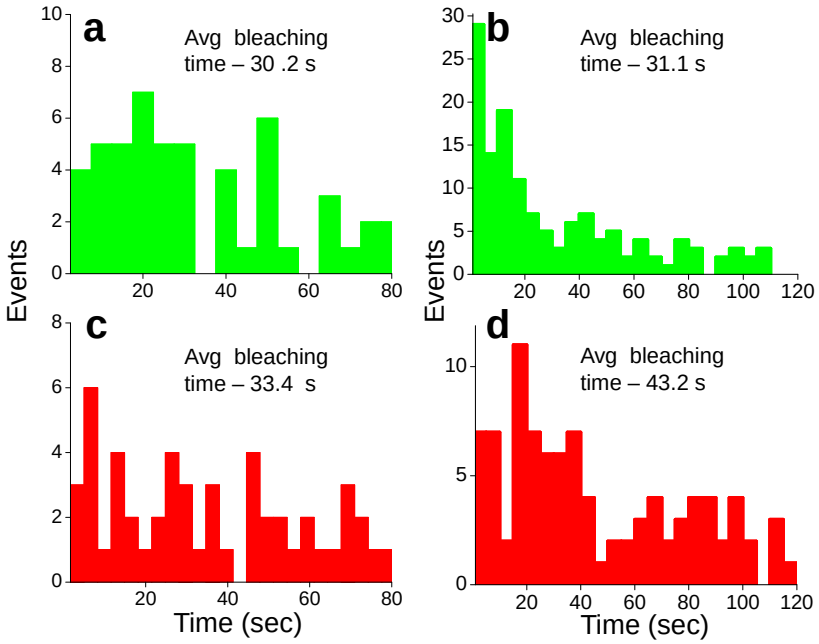

FIGURE S4. Photobleaching lifetime distributions of Cy3 and Cy5 labeled ICs on plain glass (a and c, respectively) and colocalized with small silver particles (b and d).

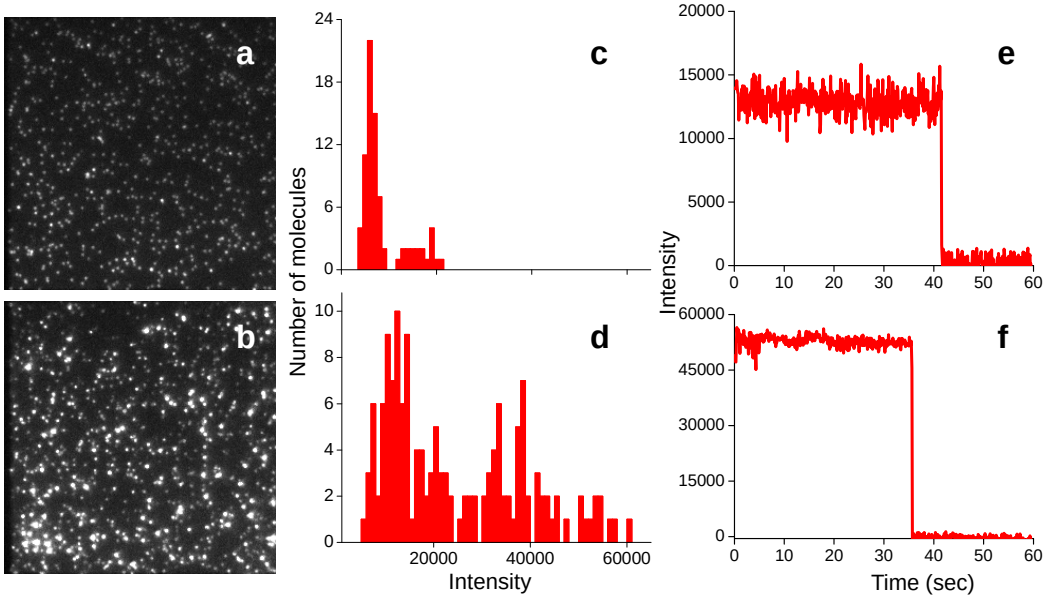

FIGURE S5. Comparison of Cy5 labeled ICs on large silver particle coated glass surface. Fluorescence images of Cy5 labeled ICs on plain glass (a) and large silver particle coated glass (b). Intensity histograms of Cy5 labeled ICs on plain glass (c) and large silver particle coated glass surface (d). Panel (c) is similar to panel (c) of Fig. S4, except that the laser intensity was higher in these experiments than for Fig. S4. Single molecule traces of Cy5 labeled ICs on plain glass (e) and a large silver particle (f).

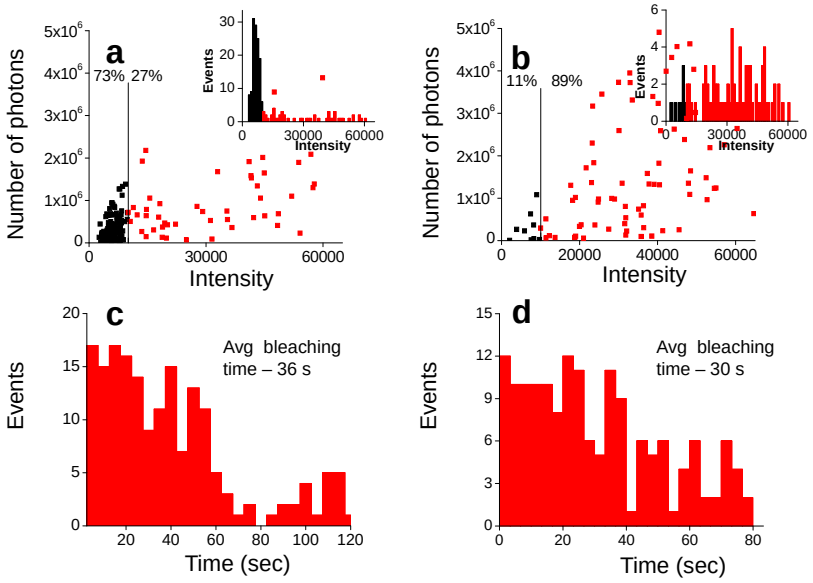

FIGURE S6. Photostability-intensity and photobleaching lifetime distribution plots of Cy5 labeled ICs on large silver particle coated glass surface**.** Number of photons emitted from each single spot before photobleaching vs. intensity of non-colocalized Cy5 labeled ICs (a), Cy5 labeled ICs colocalized with large silver particles (b). Intensity distributions for non-colocalized and colocalized Cy5 labeled ICs are in the insets of a and b respectively. Photobleaching lifetime distributions of non-colocalized (c) and colocalized (d) Cy5 labeled ICs with large silver particles.

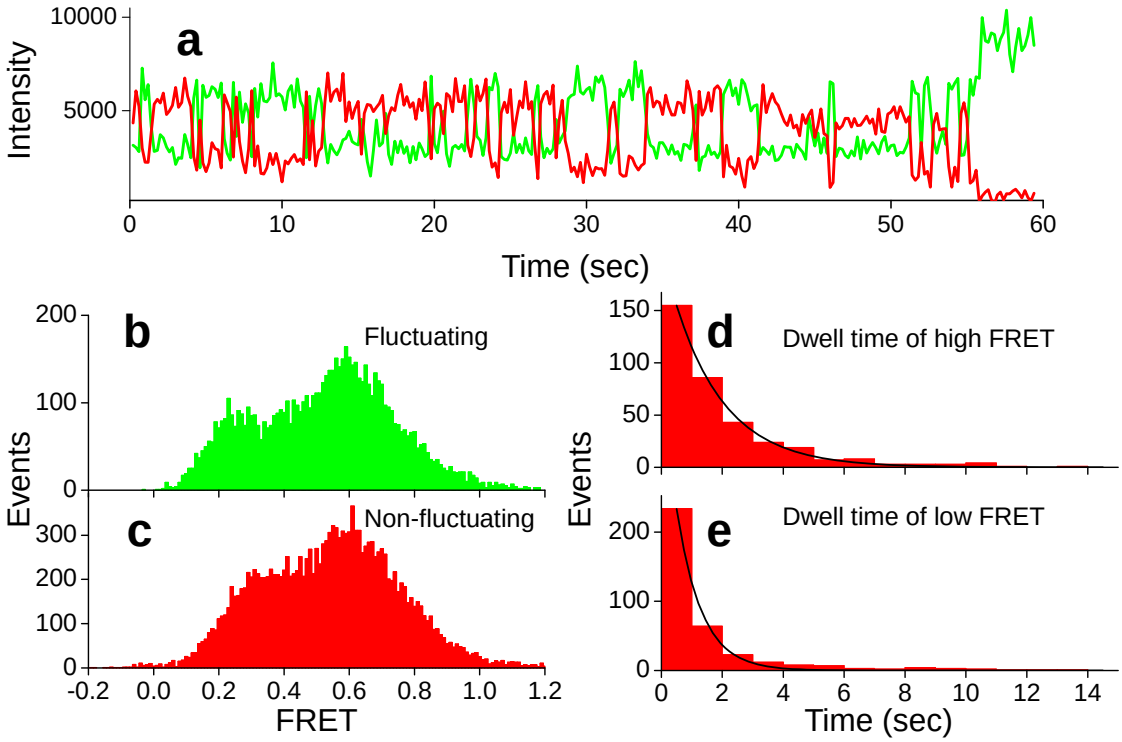

FIGURE S7. Time courses of fluorescence intensity of pre-complex (PRE-tt, having $tRNA^{Arg}$(Cy3) in P site and fMet-Arg-Phe-$tRNA^{Phe}$(Cy5) in the A site) away from particles on a small silver particle coated surface. Cy3 (green) and Cy5 (red) fluorescence intensity traces (a) under 532 nm laser illumination show fluctuations between high and low FRET and photobleaching of the Cy5 at ~55 s. FRET efficiency distributions from fluctuating and non-fluctuating complexes are shown in b and c, respectively. (d) and (e) are dwell time distributions for high and low FRET states, respectively.

References:

(1) Bike, S. G. Measuring Colloidal Forces Using Evanescent Wave Scattering. *Curr Opin Colloid Interface Sci.* **2000**, 5, 144-150.